PORT AND OCEAN ENGINEERING UNDER ARCTIC CONDITIONS
TECHNICAL UNIVERSITY OF NORWAY

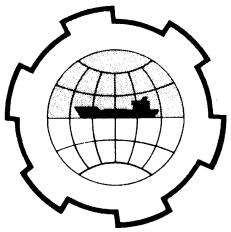

HYDRAULIC PERFORMANCE OF RUBBLE MOUND BREAKWATERS

REASONS FOR FAILURE

P. Johannesson - Research Eng. Dept. of Port and Ocean Engineering, Technical University of Norway Trondheim Norway
P.M. Bruun - Professor and Chairman

ABSTRACT

The paper discusses the hydraulic reasons for failure and makes suggestion for improvement of design. The importance of friction and permeability of core material on stability conditions is analysed. The conclusion is that the commonly used trapezoidal linear slope profile should be substituted by better reasoned design to obtain a greater degree of compatability between the wave action, slope geometry structure and cover block's geometry. A "selfadjusted" profile may be divided into three zones with different slope angle and block-characteristics and combined to achieve maximum stability.

DETAILED DISCUSSION ON REASONS FOR FAILURE

Location of failure - By model tests (1, 2) it has been found that failures at idealized sphere rubble mounds occur at or below the lowest level of wave retreat due to high normal forces. In the case of quarry stone rubble mounds with blocks placed pell mell, conditions are different. Fig. 1 demonstrates the damage distribution curves based on extensive test series (3). It was noted that damage started and was most pronounced just below S.W.L. where downrush penetrates with maximum velocity.

Pattern of failure - During intensive investigations Kydland (3) observed that the fluctuating pressure due to up- and downrush causes settlement in the armor layer particularly below S.W.L., where blocks become more closely packed. Considerable force is therefore necessary to pull or push out a block. At S.W.L. the armor blocks become less compact due to less settlement. Probably some few blocks may then have become entirely free of restraint (Fig. 2a). According to ref.

(4) and others, blocks may roll away initially in contact with its downslope neighbour (Fig. 2b) or they may in certain cases become entirely free of restraint from any neighbouring blocks and be drawn right out into the downrush. This condition was observed quite often in the laboratory, mainly with stability tests with spheres as cover layer.

The failure forces - In the case of smooth cover layers parallel forces are less pronounced and failure therefore occurs where the normal forces are maximized. In the case of rubble mounds with blocks placed pell mell, the exposed area of a protruding block may be considerable, and the moment arm for overturning forces may be relatively large. If the block moreover has no contact with its upstream neighbour, all conditions favour failure by overturning. The velocity of the downrushing water parallel to the breakwater slope, later referred to as v_p, is maximized just below S.W.L. This results in high drag and lift forces that easily may pick up a protruding block. This is fairly well demonstrated by Fig. 2.

SELFADJUSTED PROFILES

a - Relation between wave action and beach profiles characteristics. Kemp (5) found that the ratio of the duration of uprush of a wave, t_a, to the wave period, T, characterizes flow conditions on a beach. The phase difference defined as t_a/T thus enables wave and beach conditions to be classified as "surge", "transition" or "surf" condition each with its own characteristic flow pattern. The corresponding equilibrium profiles are shown in Table 1. This classification was based on the observation that for low phase differences the broken wave was able to surge up the beach to the limit of uprush, and return as backwash to the breaker point before the succeeding wave broke. The flow shoreward of the breakers was distinctly oscillatory, and the beaches steep and plane. As the height of the incident wave increases further, the crest height ceases to increase and later begins to diminish. With the retreat of the beach crest and the seaward movement of the break-point (l_b increases) the time of uprush increases. As a result the backwash is not completed before the next wave breaks. This condition involved interference between the backwash of one wave and the uprush of the next, and the oscillatory nature of the flow gave way to a transition flow regime with some increase in the interchange of water between the zones landward and seaward of the breakers.

As the phase difference was further increased to values greater than unity, the transition phase gave way to "flow" conditions in which successive breakers continually spilled water into the inshore zone, producing a corresponding return-flow. In accordance with this change in wave conditions, the step profile gradually becomes infinite and finally changes to a bar profile. After the bar profile has developed in full, the breakers become less violent, since the momentum effect of backwash is reduced.

Due to lack of space, the importance of the phase difference on run up and therefore on the stability of a rubble mound breakwater will not be discussed further in this paper. A more detailed report on this matter will be available in the near future, however.

b - Selfadjusted stable breakwater slope. The development of a stable breakwater profile under wave action shows similar characteristics. Due to the steep slope and coarse material "erosion" takes place on the upper part of the slope and accumulation of the "eroded material" takes place in the lower part.

The need for better reasoned design procedures resulting in greater degree of compatability between wave attack and cross sectional profile of rubble mound breakwaters, is pointed out in ref. (6). This again opens the possibility for use of smaller stones. Fig. 3 shows a self-formed, stabilized rubble mound breakwater as described in (6). The curvelined profile may be simplified by the three straight dotted lines, AB, BC, CD.

Similar tests were run by Popov (7) who sought information about stable profiles of earth dams in reservoirs. Fig. 4 shows a typical "abrasion profile" (7). The stable slopes have the following four characteristic zones (the heavy line 1-2-3-4-5). Zone 1-2 from maximum uprush down to the S.W.L.-line corresponds to curve A-B on the breakwater slope. Below comes a flat underwater zone (2-3 corresponding to B-C). Next comes the underwater roller zone 3-4. Below follows the accumulation zone (4-5 corresponding to CD).

The similarity of the step profile (Fig. 5a), the selfadjusted breakwater profile and the dam profiles (Figs. 3 and 4) is apparent. All profiles consist of a flat zone above and below S.W.L., which form a "false" beach. Above and below this zone follow about equally steep "underwater" and "uprush" zones. It is furthermore known that the distortion of the selfadjusted profiles $\Omega = \mu/\lambda$, where μ = vertical scale ratio and λ = horizontal scale ratio, decreases with de-

creasing size of the material forming the beach (the beach flattens). Coastal movable bed scale model relationships have been analyzed by Watts (8) and by Drs. Noda and Le Méhauté (9). These model laws, however, only apply within certain ranges of the size of the beach material (approx. 0.1-0.5 mm in diameter). They can therefore hardly be used in our case, with material of 0.6-60 mm in characteristic diameter. However, to emphasize the similarity in different beach profiles formed by waves, the step profile in Fig. 5a, a profile shown in Fig. 6a taken from Watts (Fig. 5 in (8)), and the dam profile in Fig. 4, have been modified to match the breakwater profile in Fig. 3. This is done by multiplying the vertical and the horizontal scales by a certain number.

Consider the breakwater profile as "prototype" (p) and the other profiles as "model" (m). A trial and error method of plotting the profiles then gives the data tabulated in Table 2. It is seen that the distortion as expected decreases considerably with decreasing grain size diameter-ratio ($n_D = D_m/D_p$).

Noda (9) found the following relation between $n_{\gamma'}$, λ, μ and n_D ($n_{\gamma'} = (\gamma_s-\gamma_f)/\gamma_f$ is the relative specific weight) for variation of grain size between 0.1-0.5 mm;

$$n_D \cdot N_{\gamma'}^{1.46} \quad \mu^{0.55} \tag{1}$$

$$\lambda = \mu^{1.32} \cdot n_{\gamma'}^{-0.35} \tag{2}$$

In our case $n_{\gamma'} = 1$ which reduces Eq. 1 and 2 to $n_D = \mu^{0.55}$ and $\lambda = \mu^{1.32}$. This relationship does, however, not fit the data in Table 2, except for the distortion ratio between the dam profile and the breakwater. Eq. 2 gives $\lambda = \mu^{1.32} = 3.3^{1.32} = 4.8$ which is approx. the ratio found by the plotting method. The $n_D = f(\mu,\lambda)$ relationships by Noda and Le Méhauté, however, do not apply in this case. This is indeed to be expected, because the destructive forces in case of gravel or rock fill cover material are different from those in case of a beach of fine sand. More data are needed to develop well defined model laws which apply for beach material from fine sand to gravel.

For design of breakwaters or any protecting coastal structure, it is important to note the general similarity between profiles formed by waves. A profile may be schematized by dividing it into three zones as discussed above. It is obvious however, that the hitherto commonly used trapezoidal linear slope profile, causes a very uneven distribution of forces by waves adverse to stability.

EVALUATION OF STABILITY CONDITION

Factors which affect the stability conditions of a rubble mound breakwater include; placement and size of armor layer, size of armor/sublayer, permeability of armor, sublayer and core material, friction between armor blocks and between armor and sublayer, unit weight of the armor blocks and drag, inertia and lift coefficients of armor blocks. Only the permeability of the core material and friction will be discussed in this paper.

Permeability - An important factor for the stability of a breakwater may be the porosity of the mound including filter and core material as this is a determining factor for the intensity of out- and inflow as well as for the elevation of the water table in the breakwater body, later referred to as the GW-level. For very fine core material the water table in the mound is located almost at the elevation of max. uprush, while for very coarse material the water table oscillates with and tends to follow up- and downrush.

To look more closely into the nature of the outflow, a flow net is sketched in Fig. 8 for wave conditions just before wave breaking, assuming stationary conditions for a fraction of a second. The equipotential lines may be considered as a tool to assist in drawing stream lines more accurately. The flow gradients in case of turbulent conditions must be determined by model tests. The model arrangement sketched in Fig. 9, may provide the detailed information needed to determine the distribution of flow gradients to be used for calculation of pressure and velocity field in the mound. In case of laminar flow, the velocity is expressed according to Darcy's law as $v = p_l \cdot i_l$ and as $v^2 = p_t \cdot i_t$ in case of turbulent flow. The flow net clearly reveals that the outflow is strongly concentrated at the lowest level of wave retreat, giving rise to the normal forces. p is the coefficient of permeability.

To obtain a better understanding of this, it is necessary to review the mechanics of wave breaking. Fig. 10 shows the velocity field in a breaking wave from refs. (10) and (11). While high forward velocities dominate in the crest, velocities are opposite in the toe. The rapid change in direction of velocities in the lower part of the wave, causes high acceleration fields. The condition is similar when a wave breaks on a sloping structure where downrush and outward velocities in the toe combine as indicated in Fig. 11. Phase 1, 2 and 3 in Fig. 11 are defined as follows; Phase 1: At lowest level

of wave retreat the backflow either plunges into the next wave uprush or it penetrates deep downslope before uprush by the next wave begins. Phase 2: Higher upslope the uprushing wave meets the outflow from the mound that still submerges the block. Phase 3: Still higher upslope impact forces occur when the uprush strikes an exposed block.

When downrush velocities finally meet upward velocities in the back part of the toe, the combined velocity vectors rotate causing high accelerations. This ultimately results in a broad sustained maximum of F_p, reaching a peak value as the velocity vectors are directed almost normal on the breakwater slope. At the same time F_n is maximized. This situation may be expressed as follows:

$$F_n(max) = f_1(V_n^2, \dot{V}_n, B, i, P_{gr})$$

$$F_p(max) = f_2(V_p^2, \dot{V}_p, B)$$

where V_n is the velocity perpendicular to slope intensified by outflow from the core (Fig.11 A), B is the bouyancy force, i is the flow gradient and P_{gr} is the grain pressure in the core just below the filter layer. $\dot{V}_p$ may be expressed as $\dot{V}_p = \dot{r}\dot{\phi}^2 + r\ddot{\phi}^2$ where r is the radius of angular velocity and ϕ is the angle between the r-line to the water particle in question and the breakwater slope as indicated in Fig. 11 A.

The above mentioned reveals that the highest outward normal force occurs close to the lowest level of wave retreat simultaneously as F_p is maximized. This is in agreement with observations in a number of hydraulic model tests with spheres as cover layer, but the influence of outflow on the stability (Fig. 11 A) is still uncertain. An attempt was therefore made to clarify the relative magnitude of the internal forces by laboratory experiments (12). A rubble mound breakwater was built as follows: As cover layer, spheres of 48 grammes and granit stones of 140 grammes were used respectively. The filter layer consisted of 5 grammes granit pebble while even-grained marble (4.7 - 9.4 mm in characteristic linear dimension) provided core material. Slope was 1 in 1.5. Between the armor and the sublayer various plates were placed extending down to different elevations. Three different sheets were used, one perforated, one impermeable steel plate and furthermore an impermeable plastic sheet. The results of these tests are shown in Fig. 12. It is noted that there was a very abrupt drop in height of waves causing failure when

the plastic sheet was extended down to a certain depth below S.W.L. For all alternatives tested, failure occurred at maximum downrush. The details are:

(1) Permeable steel plate between armor and sublayer. - If the permeability of the plate matches the permeability of the core material, this could be expected not to influence the inflow - outflow situation. The spheres, however, have a more even base to rest on. As shown in the Table in Fig. 12, failure at these conditions occurred for wave height of 7.5 cm (Fig. 12 a).

(2) Impermeable rigid steel plate. - As the plate reached above level of maximum uprush, the out- and inflow were limited to zone l_b in Fig. 12 b. The water table in the mound stayed just above S.W.L. instead of at elevation approximately $R_u/2$ above S.W.L. as for fully permeable tests conditions. The lower end of the steel plate was tied down. If the internal forces are of some significance, the stability could be expected to decrease when the steel plate gradually was moved downslope and the outflow became more concentrated. This was also the case, and the stability was minimized when the steel plate reached down to just below max. downrush (Fig. 12 b 2). The outflow was therefore strongly concentrated at the same place and at same time as the external forces were maximized. This resulted in a 10% reduction of wave height causing failure. As the steel plate reached further down, the stability increased again as outflow was prevented entirely (Fig. 12 b 3).

(3) In case of an impermeable flexible (no bending strength) plastic sheet, the same trend was noted and the plastic sheet did not influence the stability conditions noticeably until the plastic sheet reached down below a certain elevation when the wave height causing failure suddenly dropped approx. 50% (Table in Fig. 12).

To explain this, consider a dam with a thin asphalt or ice cover (Fig. 12 d). A certain drop in water level would induce a build up of hydrostatic pressure from the inside. In this particular case, concrete balls of 48 g placed on a 1:1.5 slope exert normal stabilizing pressure of 4.03 g/cm^2. Thus failure occurs if the outside water table drops 4 cm or more.

Comparing this to the tests with plastic sheets mentioned above, failure occurred for a wave height of 4 cm as the plastic sheet reached down to 10 cm below S.W.L. Lowest level of wave retreat was 2.7 cm. As the water level in the mound was approximately 0.7 cm above S.W.L. this resulted in maximum hydrostatic pressure of 3.4

g/cm^2 if fully mobilized which is more than 85% of the pressure necessary to push out a ball (Fig. 12 c).

Fig. 13 shows the wave situation at maximum downrush transferred from film of test series with the same ratio between maximum downrush and the elevation of the GW-level as in Fig. 12 c. Point A is the place where outflow turns into inflow. It is located 7.8 cm below lowest level of wave retreat. Using the wave profile shown in dotted lines, the equivalent point A1 is located still farther down or somewhere between elevations -7.5 cm and -10 cm as also found in the tests. When the plastic sheet reached down to or below point A, the wave height causing failure was constant and very low due to the hydrostatic pressure from the inside. The location of this out-inflow point is therefore mainly a function of the elevation of the GW-table, the wave steepness and the wave height.

The sudden, high drop in the wave height causing failure, deserves more detailed explanation. As indicated above, the wave height causing failure dropped from 8 cm to 4 cm when the plastic sheet reached down to approx. 8 cm below S.W.L. This means that point A for this particular wave condition (H = 8 cm) is located at elevation -H below S.W.L. First when the plastic sheet reached below this point, hydrostatic pressure built up. In case of a permeable steel plate placed between the armor and filter layer, the relationship between the normal forces causing failure and the wave height is assumed to follow curve 1 in Fig. 14.

In the test series one started with waves of approx. 6 cm, increasing the wave height gradually until failure occurred. The wave period was kept <u>constant</u> making the wave profile flatter for lower waves. In other words, by decreasing the wave height for a certain wave period the out-inflow point moved downslope. Build up of hydrostatic pressure in the tests therefore did <u>not</u> occur with lower wave heights.

Assume next that a flexible plastic sheet is placed between the filter and armor down to elevation 6 cm below S.W.L. Starting with very low wave heights and increasing wave height continuously, for <u>constant</u> wave steepness the relationship $F_n = f(H)$ would follow curve 2 on Fig. 14. Failure occurred for wave height of 4 cm due to build up of hydrostatic pressure. The out-inflow point A moves downslope with increasing wave height, and if failure is prevented, the force would therefore increase with increasing wave height as shown

with the dotted line in Fig. 14, until point A passes the lower end of the plastic sheet which occurs for wave height approx. 6 cm. Then hydrostatic pressure is suddenly released during wave retreat and the importance of the plastic sheet becomes almost negligible.
This evaluation might be of importance in case of coastal protection which includes impermeable mattresses of any kind as well as in case of impermeable ice sheets which may form. Consider formation of an ice sheet on a roadside or a dam due to spray action. Particularly in case of high tidal ranges, the slope might become unstable due to rather low and long waves during high tide (wind setup) if the point A is located above the lower boundaries of the impermeable sheet. One should note that the situation is most critical in zone A in Fig. 14. If the slope furthermore is built up of fine sand or silt, a small slide might initiate successive slides due to liquefaction of the fine material when the grain pressure suddenly drops. This may result in large loss of material (13).

The influence of different permeability of the core material on the stability of a breakwater, seems rather uncertain. The forces in the core which influence the stability of the revetment, may be defined as:

$$F_{core}(p) = F(v_c^2 = p \cdot i_c) + F(i_c)$$

where p is the permeability of the core material, v_c is the velocity of the water outflow from the core and i_c is the pressure gradient. The problem is now to decide the porosity that minimizes $F_{core}(p)$. To investigate the importance of permeability on the stability conditions, tests were run using the same armor layer (6 cm granite rock) and the same filter layer (2 - 3 cm stone), but with three different sizes of core material and with a wooden slab as the fourth alternative. The water elevation in the breakwater body along the S.W.L. line was measured at maximum wave run up as shown in Fig. 15. For very low permeabilities the highest water elevation occurring after max. uprush in the core just inside the sublayer, was located slightly below maximum uprush. For low permeability, hydrostatic pressure builds up in the core during wave withdrawal; $F(i_c)$ is high, $F(v_c)$ is low. It is maximized at max. downrush where the external conditions also are most critical. For high permeability of the core, the situation is opposite, because the water table in the mound follows the retreating wave more closely.

Hudson (15) and Hedar (16) found a considerable increase in stability for high permeability of the core material. In Fig. 16 the damage ratio is plotted against the wave height which demonstrates that damage was more pronounced and occurred earlier with finer core material than with a coarser core, mainly for higher damage ratios. The stability within certain limits, therefore seems to increase with increasing permeability; $F(i_c)$ is reduced more than $F(v_c)$ is increased. The damage diagram in Fig. 30 substantiates this further. It shows how the stability decreases due to build up of hydrostatic pressure in the mound when outflow is prevented. Test series I with a wood slab below the filter in Fig. 17 a is supposed to simulate an impervious core (Fig. 17 a). The wood slab however, eliminates all effects from the breakwater core. One has $F_{core}(p) = F(v_c) + F(i_c) = 0$. $F(i_c)$ is however, actually maximized when the void ratio becomes very low. Furthermore, the stability decreases when p decreases (test II, III, IV), which means that $F_c(p)$ increases, concluding in a stability condition similar to alternative I for p = 0 (wood slab, Fig. 17 a). One should, however, remember that the wood slab eliminated all effects from the core. $F_c(p)$ is therefore not maximized, but zero. The reduced stability experiment with a wood slab below the filter layer may, as discussed later, be related to a reduced angle of repose and a more intensified backwash in the zone between the wood slab and the filter layer.

Sigurdsson (1) measured the forces on spheres in an armor layer for two test series with different core material. As core material Sigurdsson used an impervious core (wood slab, series B) and a core of "infinite" permeability (open core section, series A), both with slopes 1:1.5 (Fig. 17 a, b). Quoting from Sigurdsson: "In case of an open core (series A) the intensified outflow raised the value of the maximum normal forces above and below the peak of the distribution curves. The peaks of the force distribution curves were therefore much more abrupt (steep) for series B than for series A". This may be noted by looking at the general equation for the maximal normal force per unit volume ($\forall$) given by Sigurdsson as:

$$F_n/\gamma_f \cdot \forall = \cos\alpha + \lambda H/D$$

where λ is an experimentally determined coefficient which appears to increase somewhat with increasing steepness of the breakwater and with increasing permeability of the breakwater core (decreased stability). Sigurdsson made the same assumption as in (14) and simulated

the wood slab with an impervious core. The slight increase in F_n when the wood slab ($F_c(p) = 0$) is compared to the open core section ($\Delta F_n = F_c(p=\infty) \simeq F(v_c)$, $F(i_c) \simeq 0$) indicates that the increase in drag and inertia forces on the filter and armor blocks for the model tested (Fig. 17 b) is of limited extent. $F(i_c)$ however, may be of significant magnitude as evidenced by test series II, III, IV (Fig. 16). The water tables at maximum up and downrush are sketched in Fig. 17 b. It is likely that such conditions will cause higher normal forces at lowest level of wave retreat than measured in Sigurdsson's model, which therefore gives a trend only. By comparing the results of Sigurdsson's tests and the damage diagram in Fig. 16 from test series (14), a distribution curve for forces due to inside pressure in the core versus permeability was sketched as shown in Fig. 18. Within certain limits of permeability of the core material relative to the permeability of armor and sublayer, the stability conditions are almost unaffected by small changes in the permeability. It should be emphasized that in the force-permeability diagram, the "force from the core" in case of a wooden slab below the filter layer is only used to decide the location of $F(p=\infty)$ relative to results from tests (14), Fig. 16.

Friction between the armor blocks and between armor and sublayer. Although a theoretical approach involves considerable difficulties, an attempt was made to make some calculation for dry conditions only (only internal stabilizing forces are involved). Consider an idealized sphere rubble mound with balls of weight G placed on a base, with the same roughness as the spheres (μ). Assume further that just one horizontal row (for convenience No. 1 in Fig. 19) is affected by external force (F) or by a moment (M). The corresponding stabilizing forces are shown in Fig. 20. As the unknown forces total 6 and the equations of equilibrium only 4, one still needs 2 more equations. In addition, it is assumed that one of the three frictional forces are fully mobilized at the moment of failure. Viewing the model more closely, it becomes apparent however, that the contact pressure (T_2) and the corresponding frictional forces (F_1)vanish at the moment of failure, leaving the system fully described by 4 equations.

Consider first that the external force F acts perpendicular to the mound slope contributing to following equilibrium equations for sphere No. 1 (Fig. 21 a).

$$F_y(1) \leq G \cos\alpha + S_1 + S_2 \qquad (3)$$

Equilibrium moment about points A_3 and A_0 on spheres No. 2 and 0 respectively (Fig. 21 a) gives: $S_2(max) = S_1(max) = \frac{1}{2}\ G\ \cos\alpha$ or substituted into Eq. 3:

$$\underline{F_y(max) = 2\ G\ \cos\alpha} \qquad (4)$$

F_y may be explained as the maximal stabilizing force perpendicular to the slope acting through centrum of the sphere. This may generally be expressed as (Fig. 21 b); $F(max) = 2\ G\ \cos\alpha/\cos\beta$. $M(max)$ is determined similarly by moment equilibrium about point A_3 and A_1 (Fig. 21 c) or

$$\underline{M(max) = G\ \cos\alpha \cdot D} \qquad (5)$$

where D is the diameter of the sphere. Any arbitrary force causing failure, acting on one horizontal row of spheres (Fig. 21 d), may therefore be written as $F(max) = G\ \cos\alpha \cdot D/\Delta$. It remains to determine the number of spheres (rows) above the affected sphere necessary to prevent sliding between the balls and between the balls and the base.

As seen from Figs. 20 and 21, $S_1 = S_2 = S_3 = 0.5 \cdot G\ \cos\alpha$ while $F_1 = F_2 = 0$. First one assumes that ball No. 3 (K=3) is the uppermost ball (Fig. 22). Thus the following condition is required for equilibrium; $\Sigma\ K_y(3) = 0$; $T_3 = G\ \cos\alpha + S_3$, $\Sigma\ M_c(3) = 0$; $F_3 = S_3$. No sliding at B_3 requires that $T_3 \cdot \mu \geq F_3$ while no sliding at A_3 requires that $(G\ \sin\alpha + F_3)\mu \geq S_3$ or combined

$$F_3 = S_3 \leq G\ f(\alpha)\ \frac{\mu}{1-\mu} \qquad (6)$$

where $f(\alpha) = \min|\cos\alpha, \sin\alpha|$ and $S_3 = \frac{1}{2}\ G\ \cos\alpha$. This gives the following limits for roughness (μ) resulting in stable conditions with three balls only (above the affected ball).

$$\mu \geq \frac{1}{1+2\,tg\alpha} = \mu(\alpha) \qquad \text{for } 0 < tg\alpha \leq 1 \qquad (7)$$

$$\mu > 1/3 \qquad \text{for } tg\alpha \geq 1 \qquad (8)$$

The stability conditions are sketched schematically in Fig. 23 (line $a_3 b_3 c_3$). In case of less roughness of a certain mound slope, more spheres are necessary to obtain stability. The calculations below are based on similar boundary conditions. Due to lack of space only final expressions are given. The general requirements for stability are as follows:

$$F_{3+N} = S_{3+N} = \tfrac{1}{2}\, G \cos\alpha \cdot \frac{1-(2N+1)\mu}{1-\mu(-1)^N} \qquad (9)$$

where $$\mu = \frac{1}{(2N-1)+2\mathrm{tg}\alpha} = \mu(\alpha) \quad \text{for } 0 < \mathrm{tg}\alpha \leq 1 \qquad (10)$$

$$\mu = \frac{1}{2N+1} \quad \text{for} \quad \mathrm{tg}\alpha \geq 1 \qquad (11)$$

These equations determine the number of balls (rows) necessary to prevent sliding. Failure will occur by rolling of the 3 spheres (0, 1 and 2) out of their bed, where ball 1 is affected by external forces.

Consider as an example a 1:2 mound with concrete balls as cover layer placed on a concrete plate with same roughness as the balls, $\mu = 0.1$ (Fig. 24).

Eq. 10 gives the number of spheres above the exposed sphere (No. 1) necessary to resist the maximum external force ($F_y = 2\ G \cos\alpha$) by friction of the base. One has: $2N - 1 + 2 \cdot 0.5 \geq 1/0{,}1$, $N \geq 5$. This reveals that maximum stability is obtained for ball No. 8 from the top. The maximum external forces causing failure will theoretically be constant for balls further down.

To clarify the importance of friction between cover and sublayer on the cover-layer's angle of repose (later referred to as ϕ) some dry tests were run (12). Filter blocks were glued to the wood slab (Fig. 25). The friction between cover and sublayer was changed by placing linen or plastic sheets as intermediate layers. The results are given in Table 3, where the average angle of repose, ϕ, is a function of the contact friction (later referred to as $\tau = \mu\sigma_N$) and the friction due to unevenness of the contact zone (column e in Table 3, later referred to as σ_p, p = parallel to slope) or $\phi = \phi(\tau) + \phi(\sigma_p)$.

These tests however, did not record the friction ($\tau = \mu \cdot \sigma_N$) between the armor stones and the intermediate layers. This would have required that the tests were divided in two series, one with an even stone plate below the intermediate layers and the other as described above. The first test series would then give $\phi = \phi(\tau)$ and the second, which corresponds to the tests actually run and mentioned above, gives the increase of the angle of repose due to the unevenness in the contact zone $\Delta\phi = \phi(\sigma_p)$. Column d of Table 3 gives an assumed trend of the τ-distribution with the stone against stone surfaces as reference level for friction. τ probably is maximized in the

case of the wet linen cloth because of adhesive forces. The possibility also exists that sharp edges on the cover stones may stick to the soft linen cloth.

The conclusion which may be drawn from these tests, is that the angle of repose increases with increased friction (μ) as well as with increased unevenness of the sublayer ($\phi(\sigma_p)$. This might to some extent also apply in the case of wave action. This is further in accordance with experiments run by Miller and Byrne (17). They found the following expression for the average angle of repose of a single particle on a rough bed:

$$\Phi = f(\alpha, D/\overline{K}, \beta) \qquad (12)$$

where Φ is the average angle of repose, α is a parameter which incorporates the effect of shape and roundness in particle as well as bed, $D/\overline{K}$ is the ratio of the diameter of a single grain to the average diameter of the bed grains and β is a parameter incorporating the effect of sorting of the bed grains.

Miller and Byrne carried out their experiments using uniformly sized spheres of diameter D = 0.25 mm. The results of these experiments are indicated in Table 4 and in Fig. 26 which is a diagram showing Φ as a function of D/K for various kinds of sand incl. spheres. In all cases a relation

$$\Phi = a \left(\frac{D}{\overline{K}}\right)^{-0.3}$$

was found. The figure "a" varies and increases from 50 for spheres, to 70 for crushed quartzite. In Fig. 26 the popular ratios used for subsequent layers in rubble mound by U.S. standards, have been added (ref. 18). They refer to weights which in Table 5 have been converted to grain diameter ratios. The Φ's corresponding to crushed quartzite (rubble mound block) are also listed in Table 5.

From Table 5 it may be noted that the improvement of slope stability against sliding by the use of W/10 instead of W/20 as sublayer is $\frac{1.4}{1.2} = 1.15$. The improvement of the stability by the use of a W/2 layer between the W and the W/10 layer is $\frac{1.75}{1.4} = 1.25$. With respect to spheres, a peculiar situation seems to exist. Fig. 27 shows the relation between tg Φ as found by Miller and Byrne and the number of contact points between the top spheres (armor blocks) and the sublayer spheres. Fully symmetrical and similar conditions with respect to placement of the spheres in two directions perpendicular to each other are assumed. Diameter of top armor spheres varied from 0.88 mm to

7.1 mm and diameter of bottom (sublayer) spheres was 0.25 mm. It may be noted from Fig. 27 that there is an almost linear relationship between tg Φ and the number of contact points.

In Fig. 28 the number of contact points (A) were replaced by diameters putting $A = \frac{2.56}{K}$. The following two relations were then found:

$$tg\Phi = \frac{2.61}{K} \qquad \text{for } \frac{D}{K} < 1 \qquad (13)$$

$$tg\Phi = \frac{1}{0.3+0.224\ K} \qquad \text{for } \frac{D}{K} > 1 \qquad (14)$$

The D/K > 1 situation is needless to say, the practical case for rubble mound breakwaters.

Fig. 29 is a diagram showing the relation between tg Φ and D/K with special reference to the W-ratios in practical rubble mounds. Table 6 corresponds to Table 5 referring to spheres only. From this table it may be noted that the figures indicated in column 3 are ab. 0.1 lower than the figures indicated in column 2. The maximum difference in friction angle is however, only ab. 5 degrees.

The improvement of slope stability against sliding by the use of W/10 instead of W/20 as sublayer, is $\frac{0.7}{0.6} \sim 1.15$. The improvement of the stability by the use of a W/2 layer between the W and the W/10 layer, is $\frac{0.8}{0.7} \sim 1.15$ or figures very similar to these valid for the quartzite grains (blocks). This situation should be kept in mind whenever sliding is assumed to become the major danger to stability.

Other interesting details should be noted. In ref. (18) the U.S. Army Corps of Engineers warns against the use of only one layer of armor blocks because this lowers the safety factor and increases the risk of collapse of the entire design by removal of the armor layer. From Table 6 it may be noted that tg Φ for W/W (two layers of weight W), is 1.1 (3rd column of Table 6) while for $W/\frac{W}{10}$ it is 0.7 only. It has occasionally been recommended to place a W/2 layer between the W and the W/10 layer. The advantage of this is obvious from Table 6. The $W/\frac{W}{2}$ is 0.95 and the $\frac{W}{2}/\frac{W}{10}$ ratio is 0.8 compared to 0.7 for the $W/\frac{W}{10}$ ratio.

Wave attack - The question is now whether one can compare the following two conditions directly:

a) dry condition where failure is caused by sliding which means that the stability = f (angle of repose).

b) wet condition under wave action when failure is mostly caused by lift and/or overturning forces. A solid "toesliding" does not occur until higher damage ratios are reached.

Looking back at the results of test series 12 a comparison between the angle of repose (dry conditions) from Table 3 and the damage diagram from the previously mentioned stability tests with quarry stones as cover layer (Fig. 30), seems to reveal the importance of friction between armor and sublayer for the stability of a quarry stone breakwater. This may be noted from the fact that the stability is higher when a linen cloth is put in between armor and filter than it is for the common rubble mound (curve 2). This in turn indicates that the internal forces are of limited order when the lower end of the impervious layer is kept above a certain elevation (curve 1, 2, 3). The increased stability in case of wave attack (curves 3 - 2 - 1 in Fig. 30) therefore seems to be related to the higher angle of repose (increased "friction").

In case of a cover layer of spheres (Fig. 31) one could however, expect that model effects would be more pronounced, which means that the angle of repose for spheres decreases with increasing unevenness of sublayer. This seems however, not to be the case. A more uneven sublayer increases the unevenness of the cover layer ($d\phi$ increases), but simultaneously contact pressure in the armor layer is reduced (N decreases). Table 7 compares the wave height causing failure in case of armor layer consisting of spheres and the angle of repose for a sheet of quarry stones placed on the same sublayer. A remarkable increase in stability with increasing unevenness is noted just as for the quarry stone tests in Fig. 30. The stability in case of wave action therefore seems to increase with increasing angle of repose (Φ) for dry conditions. That Φ increases with increasing unevenness, even for spheres, may be explained as follows. Φ is a function of the contact pressure between the spheres (N, Fig. 31) and the angle between the force direction and the slope ($\Delta\phi$). Φ therefore may be expressed statistically as follows, $\Phi = f(\Delta N_{m!})$, where $\Delta N_n = \Delta\phi_n \cdot N_n$ and $N_n = f(\sum_1^n G \cos\alpha, 1/\Delta\phi_n)$. $n = 1, 2, ...m$, where m is total number of spheres on the slope.

The conclusion is that for dry conditions the angle of repose for quarry stones as well as for spheres as cover layer increases with increasing unevenness of the sublayer. The stability in case of wave attack seems to increase with increasing angle of repose for dry conditions.

DISCUSSION AND CONCLUSION

As previously mentioned, failures for a quarry stone rubble mound are concentrated close to S.W.L. Forces causing failure are mostly drag and lift forces derived from the downrushing water (external forces) while forces from outflow are less important. The relatively small importance of porosity and the great influence of (uniform) placement, are indicative for this situation. It is therefore of importance to minimize the area of the blocks which induces parallel drag and lift forces. This requires the best possible uniform placement of the cover layer which theoretically may be obtained for shperes placed on an even sublayer. In case of spheres as cover layer, failure occurs however, by wave heights causing destructive normal and parallel forces at or below lowest level of wave retreat. For a cover layer of spheres, drag and inertia coefficients at the "max-downrush" zone must therefore be minimized to give same stability conditions as in the S.W.L. zone. This applies to external drag, lift and inertia forces occuring as a result of the velocity field in the toe of the wave as well as drag forces from the backwash and the outflow.

Due to such local failures on a straightlined breakwater profile, one may, based on analyses of selfadjusted "beaches", divide the rubble mound slope for design and construction, into three zones, each with its characteristic block properties (Fig. 32). The "false" beach, BC, evolves a new breaking point at C and changes the waves to a plunging type which reduces the run up due to turbulence and out-of-phase damping between uprush and downrush. The breaking wave does not strike the exposed breakwater slope, but plunges into water in front of the breakwater and then rushes up the slope as a bore. The steep slope, CD, separates backwash from the retreating velocity field in the downrush at the toe of the breaking waves, and therefore makes the backwash - incipient breaker interaction less violent. This reduces the maximum normal as well as the parallel forces at the lowest level of wave retreat. These forces usually are the most critical forces for the stability of a breakwater. Furthermore the layer, HG, with low permeability prevents outflow to be concentrated at the breaking point, where the external forces are maximized.

The upper layer, FE, with lower permeability prevents inflow above point E which reduces build up of hydrostatic pressure in the mound during wave retreat. This layer however is not considered fundamental for stability. The HG and FE layers may e.g. be nylon sheets.

In zone BC, drag coefficient of the blocks parallel to the slope and the exposed area of armor blocks, should be minimized. In zone CD, drag coefficient of the armor blocks perpendicular to the slope should be minimized due to the high normal forces and the concentrated outflow.

Such properties may be aimed at for a breakwater or any structure exposed to waves. It provides the benefits of adaptability of the armor blocks and "beach" profile to the external wave conditions. The wave forces are reduced (damping, turbulence) and more evenly distributed resulting in more economical design.

It is believed that further research on stability of rubble mound breakwaters should be concentrated on measurements of the wave force distribution along the exposed slope as well as simultaneous photographic records of the water table. With known permeability of the rubble mound material a mathematical model may be developed to distinguish between forces of hydrostatic as well as dynamic nature and to determine the inflow - outflow distribution along the slope during one uprush - downrush cycle.

REFERENCES

(1) Sigurdsson, G. "Wave forces on breakwater capstones". Waterways and harbors division, August 1962, WW3.

(2) Johannesson, P. "Wave forces on breakwater slope", The Technical University of Norway, Trondheim, Norway 1970. Unpublished.

(3) Kydland, O. "Stabilitet av rausmoloer. - Virkning av steinens egenvekt". Thesis for the degree of Licentiatus Technicae, Main Library of the Technical University of Norway, Trondheim, Norway 1966.

(4) Brandtzæg, A. "The effect of unit weights of rock and field on the stability of rubble mound breakwaters". The Xth Conference on Coastal Engineering in Tokyo 1966.

(5) Kemp, P.H. "The relationship between wave action and beach profile characteristics". Seventh Conference of Coastal Engineering, The Hague, Netherlands, August 1960, Vol. I.

(6) Priest, M.S.
Pugh, J.W.
Singh, R. "Seaward profile for rubble mound breakwaters". Ninth Conference of Coastal Engineering, Lisbon, Portugal, June 1964.

(7) Popov, I.J. "Experimental Research in Formation by Waves of Stabile Profiles of Upstream Faces of Earth Dams and Reservoir Shores". Seventh Conference of Coastal Engineering, The Hague, Netherlands, August 1960, Vol. 2.

(8) Watts, G.M. "Laboratory Study of Effects of Varying Wave Periods on Beach Profiles". Technical Memorandum No. 53, September 1964.

(9) Noda, E. "Coastal Movable-Bed Scale Relationship". Tetra Tech Inc., Pasadena, California 91107, March 1971.

(10) Iversen, H.W. "Laboratory Study of Breakers, Gravity Waves". National Bureau of Standards Circular 521, Washington D.C., 1952.

(11) Miller, R.L. Zeigler, J.M. "The Internal Velocity Field in Breaking Waves". Ninth Conference of Coastal Engineering, Lisbon, Portugal, June 1964.

(12) Loe, H. "The Influence of Impermeable Sheets Placed Below the Armour on the Stability of Rubble Mounds". The Technical University of Norway, Trondheim, Norway, 1969. Unpublished.

(13) Bjerrum, L. "Subaqueous Slope Failures in Norwegian Fjords". Conference on Port and Ocean Engineering under Arctic Conditions, Technical University of Norway, Trondheim, Norway, August 1971.

(14) Bruun, P.M. "Damage Functions of Rubble Mound Breakwaters". Discussion in Waterways and Harbors Division, WW2, May 1970.

(15) Hudson, R.Y. "Laboratory Investigation of Rubble Mound Breakwaters", Transactions of the ASCE, 1961, Vol. 126, Part IV.

(16) Hedar, P.A. "Stability of Rock-fill Breakwaters", Akademiförlaget-Gumperts, Gøteborg 1960.

(17) Miller, R.L. Byrne, R.J. "The Angle of Repose of a Single Grain on a Fixed Rough Bed", Technical Report No. 4, Department of the Geophysical Sciences, the University of Chicago, May 1965.

(18) Jackson, R.A. "Design of Cover Layers for Rubble Mound Breakwaters Subjected to Nonbreaking Waves", Research Report No. 2-11, US Army Engineering Waterways Experiment Station, Vicksburg, Mississippi, 1968.

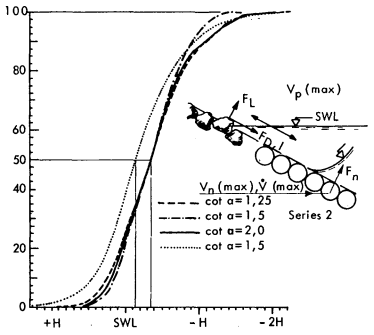

FIG. 1 - CUMULATIVE DISTRIBUTION OF DAMAGE ALONG THE BREAKWATER FACE (4) SERIES 1 AND 2.

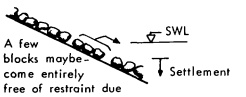

A few blocks maybe-come entirely free of restraint due to the settlement of armor below SWL (6)

FIG. 2a - START OF FAILURE

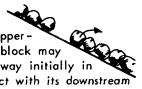

The upper-most block may roll away initially in contact with its downstream neighbour (4). Failure therefore occurs where the internal stabilizing forces are minimized.

FIG. 2b - START OF FAILURE

TABLE 1

SHORT TERM VARIATION BEACHES - "EQULIBRIUM PROFILE"

Surge conditions	Transition conditions	Surf conditions
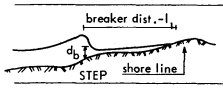	Beach cups are developed by the three dimensional flow pattern	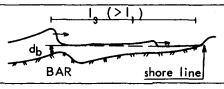
Summer - shingle beaches Ho/Lo < 0.02 - 0.03	Unstable transition zone for the phase difference ratio ≃ 0.02 - 0.03	Winter, storm - sand beaches Ho/L > 0.02 - 0.03
SURGE	The transition from step to bar type profile is fully achieved once surf conditions are established → SURF Thus H_b critical (step-bar) is a function of the ware period,) : $H_b(Cr) \sim T$	
Beach profile dim. vs. wave charachteristic	$l \sim \sqrt{H_b}$	$l = K \cdot H_b \cdot \sqrt{H_b/D}$

$H_b \sim D \sqrt{\cot \alpha}$ where α is the beach slope.

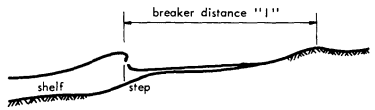

FIG. 5a - TYPICAL STEP PROFILE

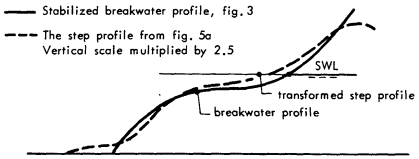

FIG. 5b - BREAKWATER PROFILE (FIG. 3) AND TRANSFORMED STEP PROFILE FROM FIG. 5a.

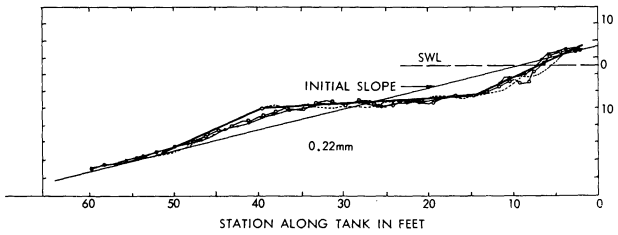

LEGEND
Mean wave period 2.00 sec.
Period varied ± 10% from mean period, period changed every 10 minutes
" " " " " " " " " hour
Constant period test (2.00 sec.)
Test time = 40 hours

FIG. 6a - EFFECT OF FREQUENCY OF PERIOD VARIATIONS, WATTS (8) 1954

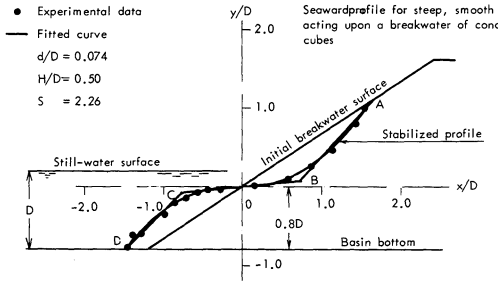

FIG. 3 - STABILIZED BREAKWATER PROFILE (6)

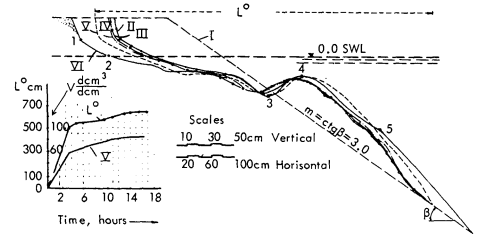

Different stages of formation by waves of stable profiles. Gravel with grain diameter, d_{60}=6 mm. Wave parameters: H = 30 cm, L = 4.5 m, T = 1.73 sec.

I - orginial slope
II - profile after 3.6 hours
III - - - - - 4.8 -
IV - - - - - 6.0 -
V - - - - - 9.6 -
VI - - - - - 16.8 -

L^{o}= slope lenght, cm
V = volume of erosion, dcm^3/dcm

FIG. 4 - EXPERIMENTAL RESEARCH IN FORMATION BY WAVES OF STABLE PROFILES OF UPSTREAM FACES OF EARTH DAMS AND RESERVOIR SHORES (7).

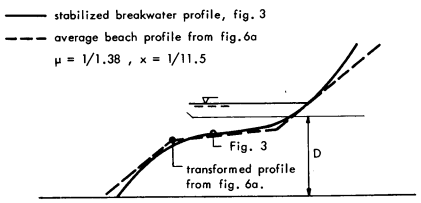

FIG. 6b - BREAKWATER PROFILE (FIG.3) AND TRANSFORMED STEP PROFILE FROM FIG. 6a.

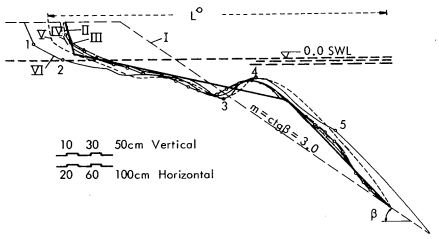

FIG. 7a - MODIFIED DAM PROFILE FROM FIG. 4 USED IN FIG. 7b.

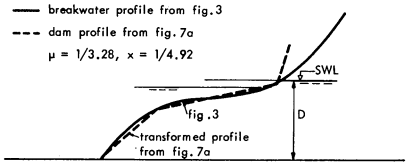

FIG. 7b - BREAKWATER PROFILE (FIG 3) AND TRANSFORMED MODIFIED DAM PROFILE (FIG. 7a).

Table 2

	Grain size D in mm	Grain size ratio n_D	Horizontal scale ratio λ	Vertical scale ratio μ	Distortion Ω = μ/λ
Rubble mound breakwater	313	1	1	1	1
Dam (Fig. 7a)	0.6	0.2	4.92	3.3	0.66
Beach profile from Watts (Fig. 6a)	0.22	1/141	11.5	1.38	0.12
Step profile (Fig. 5a)	0.1	1/313	2.5	1	

FIG. 8 - FLOW NET IN CASE OF STATIONARY CONDITIONS AT MAXIMUM DOWNRUSH

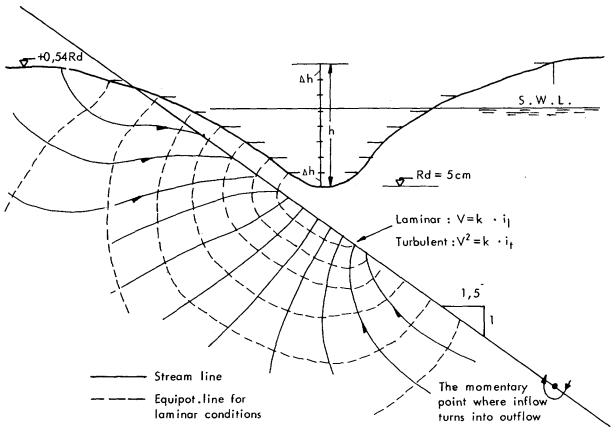

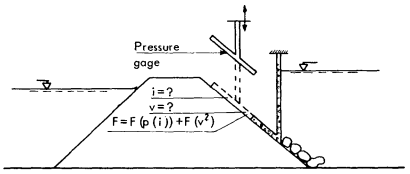

FIG. 9 - MODEL CROSS SECTION OF SIMILITUDE FOR DECITION OF FLOW GRADIENTS AND VELOCITIES

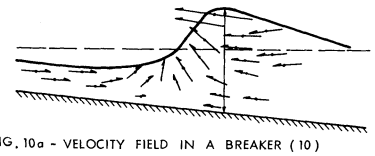

FIG. 10a - VELOCITY FIELD IN A BREAKER (10)

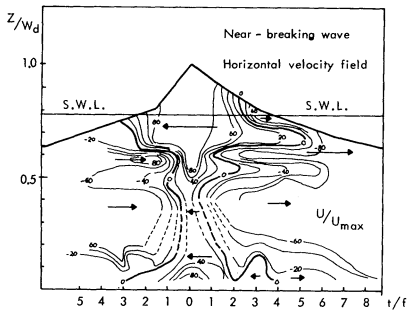

FIG. 10b - WAVE PROFILE NEAR BREAKING AND RELATIVE VELOCITY FIELD ACCORDING TO (11)

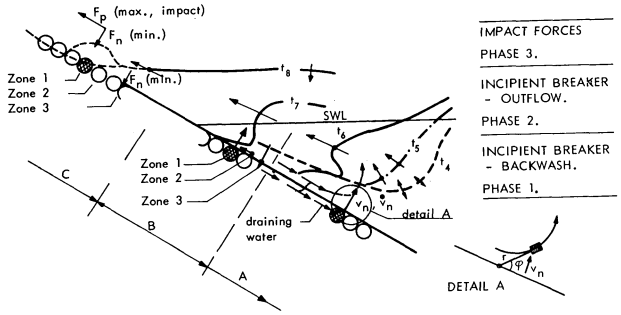

FIG. 11 - FORCE DISTRIBUTION FOR PHASE 1, 2 AND 3.

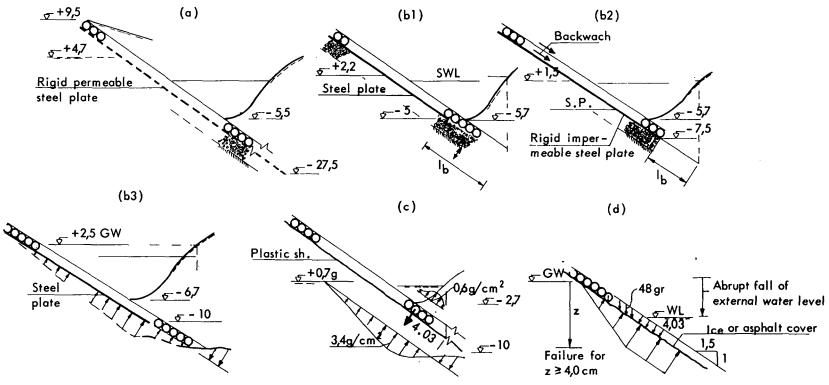

TABLE		WAVE HEIGHT CAUSING FAILURE				
	Elevation of lowermost end of int. layer	±0	-5	-7,5	-10	-27,5
a	Perxorated steel pl.					7,5
b	Imperm. steel pl.	8,4	8,2	7,2	8,5	8,0
c	Flexible plastic pl.	7,8	8,0	7,2	4,0	4,1

FIG. 12 - STABILITY TESTS WITH AN INTERMEDIATE LAYER BETWEEN ARMOR AND SUBLAYER

FIG.13 - FLOW NET AND DISTRIBUTION OF OUTFLOW GRADIENTS FOR "STATIONARY CONDITIONS" AT MAXIMUM DOWNRUSH. SLOPE 1 : 1,25. LOCATION OF POINT OF 'OUTFLOW - INFLOW'.

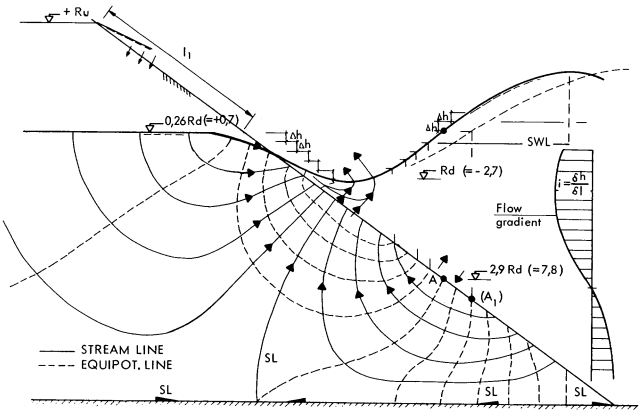

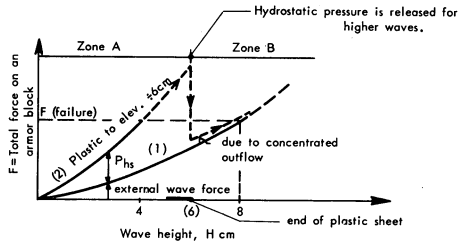

FIG. 14 - DISTRIBUTION OF FORCES CAUSING FAILURE AT MAXIMUM DOWNRUSH WITH AND WITHOUT AN INTERMEDIATE FLEXIBLE LAYER ($\sigma_b = 0$) BETWEEN ARMOR AND SUBLAYER.

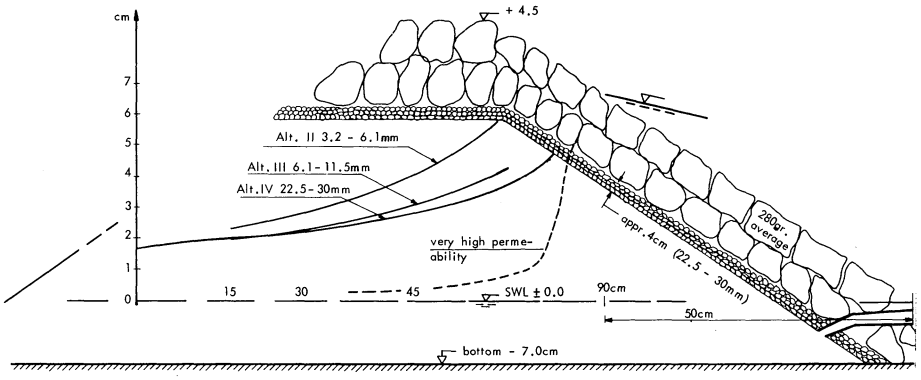

FIG. 15 - WATER ELEVATION IN THE CORE AT MAXIMUM UPRUSH FOR VARYING PERMEABILITY OF THE CORE

Note: Damage is more pronounced and occurs earlier for finer core material (alt. II) than with a more coarse core, mainly for higher damage ratios. P = coefficient of permeability. Armor was 6 cm in diameter.

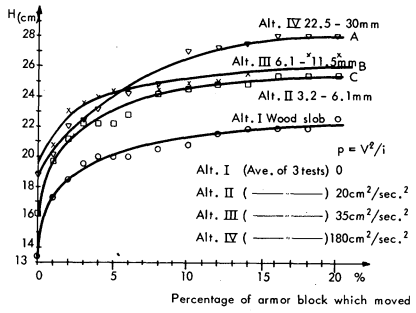

FIG. 16 - DAMAGE RATIO VS. WAVE HEIGHT FOR DIFFERENT CORE MATERIAL (14)

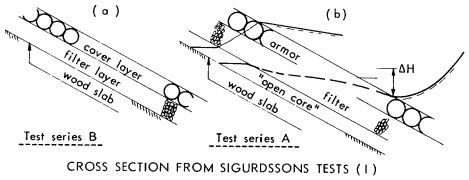

CROSS SECTION FROM SIGURDSSONS TESTS (1)

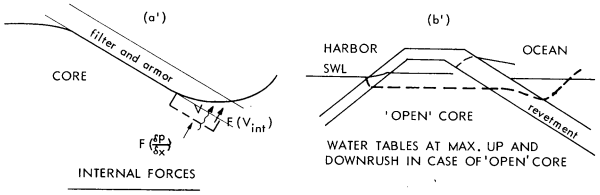

FIG. 17 - THE IMPORTANCE OF THE PERMEABILITY OF THE CORE MATERIAL ON THE STABILITY CONDITIONS

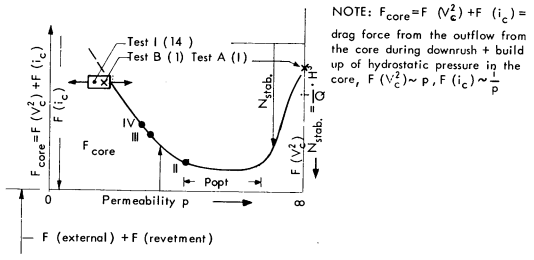

FIG. 18 - PERMEABILITY OF CORE MATERIAL VS. BREAKWATER STABILITY

G = weight of sphere
α = breakwater slope
μ = coefficient of friction

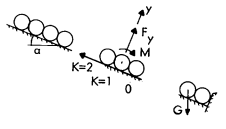

Note: One horizontal row of spheres No. 1, is affected by an external force (F_y) or moment (M).

FIG. 19 - DEFINITION OF SYMBOLS

Note: At the moment of failure the contact pressure between the affected sphere and the base becomes zero (statically determined system) which in turn means, (neglecting the dynamic effects), that $S_1 = S_2$

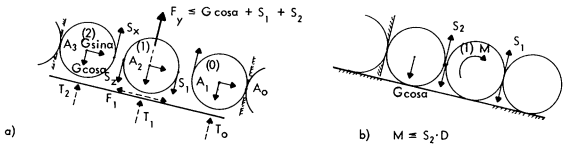

At the moment of failure $T_1 = T_2 = T_0 = 0$

$F_1 = F_2 = F_0 = 0$

$S_2 \rightarrow S_1$

FIG. 20 - DEFINITION OF STABILIZING FORCES

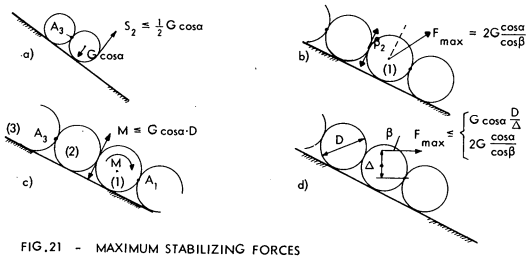

FIG.21 - MAXIMUM STABILIZING FORCES

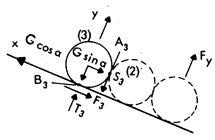

FIG. 22

Calculation of number of spheres above the affected sphere necessary to prevent sliding between the balls and between the balls and the base (admits full mobiliazation of the torque moment

First one calculates the slope angle (abscissa) and the coefficient of friction (μ - ordinat) for stable condition for $K = 3$ ($F_3 = S_3$)

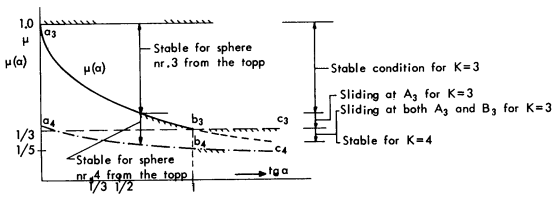

FIG. 23 - NUMBER OF BALLS NECESSARY TO STABILIZE THE TORQUE MOMENT VS. SLOPE CHARACTERISTICS

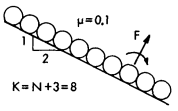

Consider as example μ=0.1, cotα=2. F_y increases and is maximized for ball No. 8, F=const. for $K \geq 8$.

FIG: 24 - F_y(max) DISTRIBUTION

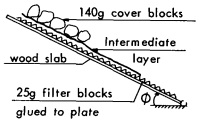

In test series (12) the angle of repose, for dry conditions, was found for different friction conditions (by means of an intermediate layer) between filter and armor layer. The results are shown in Table 3 .

FIG. 25 - CROSS SECTION OF MODEL, Φ_{max} = ANGLE OF REPOSE

TABLE 3 INTERMEDIATE LAYER		(a)	Angle of repose Ø (b)	Contact zone (c)	Ø(T) (d)	Ø=Ø(σ_p) (e)
1	"	Linen sheet	59.5°	Stone/Linen	+	little more even (-)
2	Uneven surface	Directly on filter	52.7°	Stone/Stone	0	0
3		Plastic sheet	43.6°	Stone/Plastic		more even
4	Smooth	Wooden plate	37.6°	Stone/Wood	(+)	
5	surface	Perf. metal plate	35.2°	Stone/Metal	0	

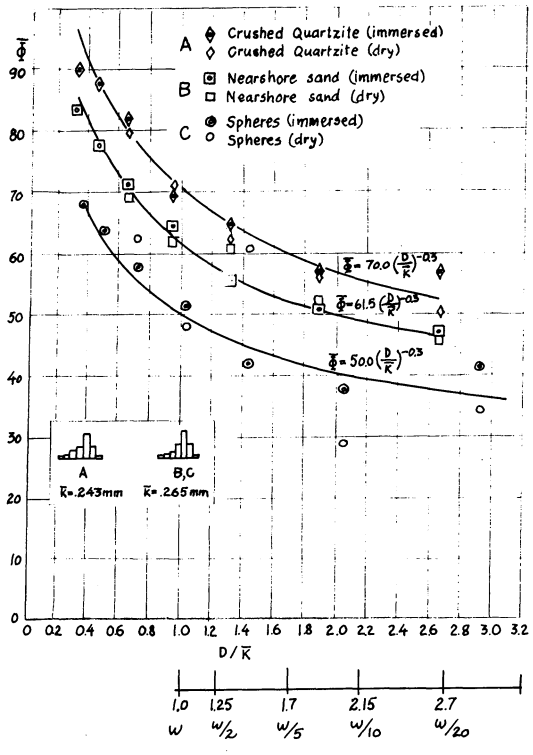

FIG. 26 - $\bar{\Phi}$ AS FUNCTION OF THE D/$\bar{K}$ RATIO (ref.17)

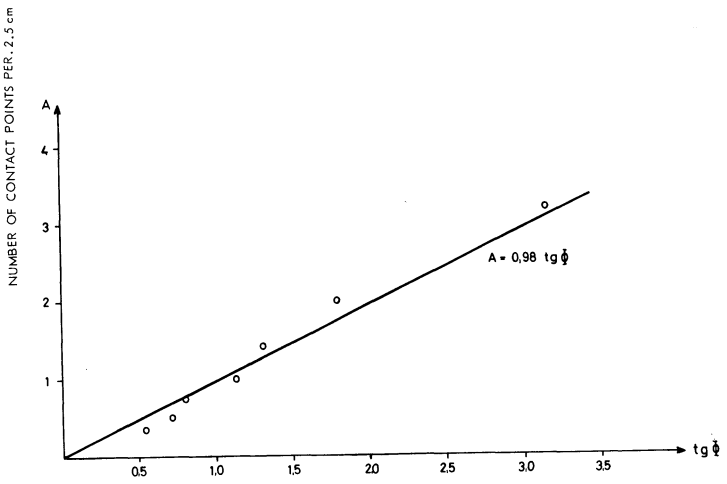

FIG. 27 - RELATION BETWEEN NUMBER OF CONTACT POINTS BETWEEN SPHERES AND tan Φ

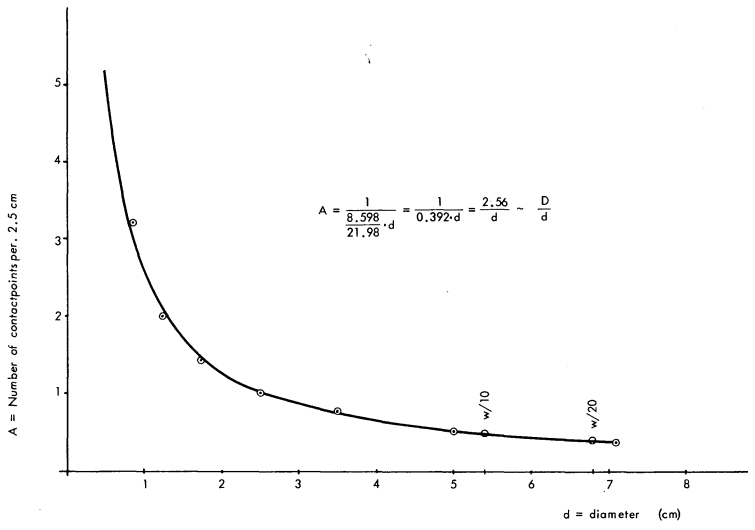

FIG.28 - NUMBER OF CONTACT POINTS BETWEEN STONES VERSUS GRAIN DIAMETER.

Table 4 Angle of repose of individual spheres on fixed bed of uniformly sized spheres of diameter, K = .250 mm.

Particle Size D	.088 mm	.125	.175	.250	.350	.500	.710 mm
$\bar{\Phi}$	72.4°	61.1°	52.5°	48.6°	38.5°	35.7°	29.0°
σ_Φ	16.9°	5.2°	14.0°	18.5°	19.0°	15.8°	9.7°
Tan $\bar{\Phi}$	3.152	1.804	1.303	1.134	0.795	.719	0.554
$D/\bar{k}$	0.352	0.500	0.700	1.000	1.400	2.000	3.000

Table 5 Popular weight ratios in rubble mounds and the corresponding ratios between diameters in armor and sublayers, Φ's and tg Φ (approximately) for crushed quartzite

Weight ratios	Diameter ratios	Φ	tg Φ
W to W	1	70°	2,75
W to W/2	1,25	65°	2,1
W to W/10	2,15	55°	1,4
W to W/20	2,7	50°	1,2
W/2 to W/10	1,7	60°	1,75
W/2 to W/20	2,15	55°	1,4

Table 6 Popular weight ratios in rubble mounds and the corresponding ratios between diameters in armor and sublayer, Φ's for spheres according to Fig. 26 and to Fig. 29.

Weight ratios	tg Φ (Fig. 26)		tg Φ (Fig. 29)	
W to W	1,2	(50°)	1,1	(48°)
W to W/2	1,05	(47°)	0,95	(43°)
W to W/10	0,85	(40°)	0,7	(35°)
W to W/20	0,7	(36°)	0,6	(31°)
W/2 to W/10	0,9	(38°)	0,8	(39°)
W/2 to W/20	0,85	(40°)	0,7	(35°)

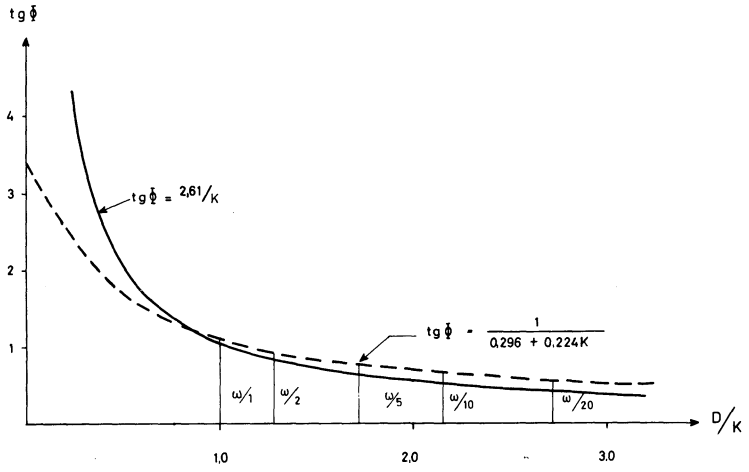

FIG. 29 - RELATION BETWEEN tg Φ AND D/K

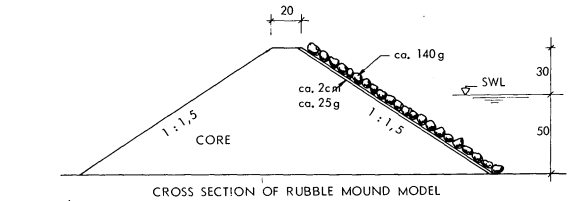

CROSS SECTION OF RUBBLE MOUND MODEL

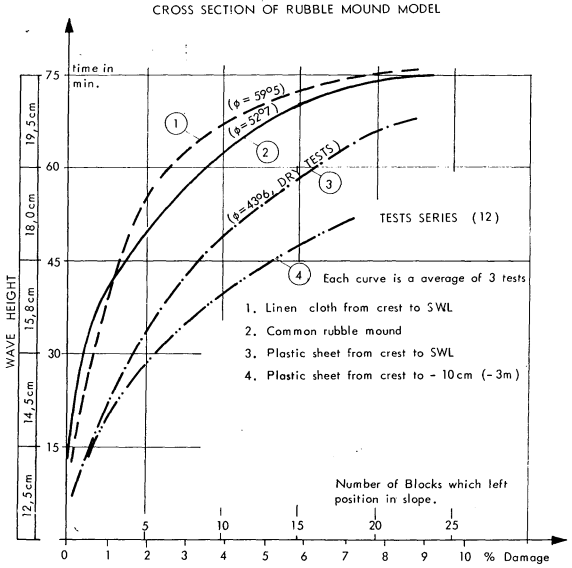

FIG. 30 - WAVE HEIGHT VS. DAMAGE RATIOS

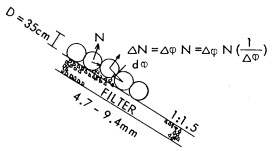

A more uneven sublayer increases the unevenness of the cover layer (dφ increases), but simultaneously contact pressure in the armor layer is reduced (N decreases). This results in more stable conditions, according to Table 3 and Fig. 30.

FIG. 31 - INFLUENCE OF UNEVENNESS OF ARMOR LAYER CONSISTING OF SPHERES ON THE ANGLE OF REPOSE.

TABLE 7.	Failure wave height for spheres	Angle of repose for quarry stone
Perforated steel plate	H_f = 9.0 cm	$\phi = 35.2^o$
Plastic sheet	H_f = 9.5 cm	$\phi = 43.6^o$
Directly on the subl.	H_f = 10.0 cm	$\phi = 59.5^o$

Note: The wave height causing failure seems to increase with increasing angle of repose.

FIG.32 - OPTIMALIZATION OF BREAKWATER PROPERTIES

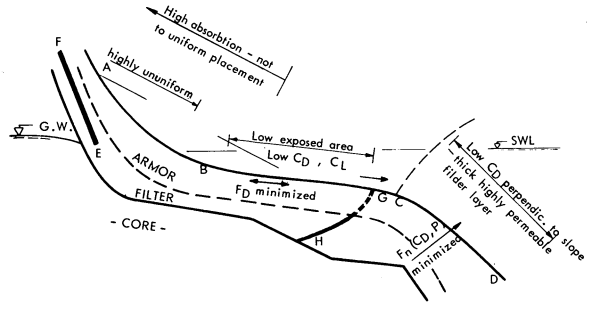

The 'false' beach, BC, evolves a new breaking point at C, which reduces run up (plunging waves and out of phase damping ($t_a/T/2$)).

The impervious layer, FE, prevents inflow above point E which reduces the build up of hydrostatic pressure in the mound. The impermeable layer, GH, prevents backwach - outflow to be concentrated at the breaking point, where the external forces are maximized.

The steep slope, CD, makes the backwash - incipient breaker interaction less violent and further separates backwash from the retreating velocity field in the toe of the breaking wave.

The breakwater slope is divided into three zones, each with its characteristic block - properties. This results in more evenly exposed structure which increases safety against failure. In all cases, however, some flexible interlocking effects is very significant.